IMT Mines Albi-Carmaux
École Mines-Télécom

STUDY REPORT

FROM THE SPARK TO THE FLAME

STUDY OF THE PLASMA CHEMICAL KINETIC EFFECT ON IGNITION BY MAKING A DIRECT NUMERICAL SIMULATION ON A PIN-PIN CONFIGURATION

Pierre CHAMPEIX
IFIE EAE 2017

CERFACS

CENTRE EUROPÉEN DE RECHERCHE ET DE FORMATION AVANCÉE EN CALCUL SCIENTIFIQUE

Mines's supervisor
Sylvain SALVADOR

CERFACS's supervisors
Bénédicte CUENOT
Olivier VERMOREL
Félix COLLIN-BASTIANI

March-August 2017

1 Acknowledgements

First, I would like to express my special thanks to Benedicte CUENOT and Olivier VERMOREL who allow me to do this internship at CERFACS. Then, I also thank Felix COLLIN-BASTIANI with who I worked during my entire internship.

I also thank Sylvain SALVADOR for his help and his advices during all my internship and specially for the help he gave me for the internship defense.

Moreover, I also thank the CFD team of CERFACS for their punctual helps during my work especially Robin CAMPET, Majd DAROUKH, Maxime FIORE, Valentin JONCQUIERES, Dario MAESTRO and Luc POTIER.

Finally, I thank all other interns who made their internship with me and with who it was pleasant to work.

Contents

2   Abstract

This study takes place into the ANR project called FAMAC for Fondamentaux d'Allumage pour Moteurs à Allumage Commandé. The aim of this project is to better understand the early stages of spark ignition in order to offer innovative solutions for better performances. The understanding and control of the ignition process aim for reducing pollutants and for extending the working limits of internal combustion engines.

The aim of this work is to study the effect of the plasma chemical kinetic on ignition. During the ignition process, high temperatures are reached (>50 000K) and a plasma, i.e. a ionized gas, is created. At such high temperatures, important chemical effects need to be taking in account such as dissociations and recombinations.

To study these effects, Direct Numerical Simulations of two different discharges using the academic anode-cathode configuration in pure air and in a propane/air mixture of $\phi = 1$ are presented. For both discharges, two cases are considered: a first one plasma chemistry and a second one without plasma chemistry, i.e. considering combustion chemistry only. To model the plasma, an energy deposition model is used.

Results show a direct influence of the plasma chemistry on the peak of temperature of the plasma with a difference of more than 1000K for a discharge in pure air. This difference is mostly due to the dissociation of the dioxygen and of the dinitrogen in the plasma which are endothermic reactions. Moreover, results are compared to experimental data and show a good agreement. However, there are some discrepancies in the temperature evolution microseconds after the beginning of the discharge in pure air. Those differences are due to the energy deposition model that needs to be improved.

3   Résumé

Cette étude s'inscrit dans le projet FAMAC(Fondamentaux d'Allumage pour Moteurs à Allumage Commandé) de l'ANR. Le but de ce projet est de mieux comprendre les premiers instants de l'allumage par étincelle pour pouvoir obtenir des solutions innovantes et de meilleures performances. En effet, la compréhension et le contrôle du processus d'allumage permettent de réduire les polluants et d'étendre les limites d'utilisation des moteurs à combustion interne.

Le rôle de ce travail est d'étudier les effets de la cinétique chimique du plasma sur l'allumage. Durant l'allumage, un plasma est créé et peut dépasser les 50 000K. A de telles températures, d'importants effets chimiques sont à prendre en compte comme les dissociations ou les recombinaisons des espèces.

Pour étudier ces effets, des simulations numériques directes de deux décharges ont été effectuées en utilisant la configuration académique de l'anode-cathode. La première simulation est une décharge dans l'air pur, la seconde est une décharge dans un mélange air-propane de richesse $\phi = 1$. Pour ces deux simulations, deux cas sont étudiés. Un premier en considérant aucune chimie du plasma and la seconde en la considérant. Pour modéliser l'allumage par bougie, un modèle de dépôt de l'énergie est utilisé.

Les résultats montrent une influence directe de la chimie du plasma sur les pics de température avec une différence de plus de 1000K pour la décharge dans l'air pur. Ces différences sont principalement dues aux dissociations du dioxygène et du diazote dans le plasma qui sont des réactions endothermiques. De plus, les résultats sont comparés aux données expérimentales et montrent de bons accords. Cependant, quelques différences dans l'évolution temporelle de la température sont visibles quelques microsecondes après le début de la décharge. Ces différences sont dues au modèle du dépôt d'énergie. Des nouvelles calibrations doivent être effectuées ou alors certaines hypothèses doivent être modifiées.

4   Introduction

Nowadays, within the current environmental context, important efforts are made by the car industry in order to limit pollutant emissions. One aspect which can be improved is the ignition process and a better understanding of it offers innovative solutions for better performances. The FAMAC project is in charge of this study and this work is a part of this project.

The ignition process for an academic anode-cathode configuration is divided in three main parts. The first part is following the electric discharge with the formation of a hot gas kernel at the spark plug. Then, the second part is the growth and the propagation of the hot gas kernel up to the nearest fuel injector. Finally, the third part is the propagation of the flame. This study only focuses on the first part. This step occurs at very small scales which allows to used DNS to get a better understanding of the main mechanisms of this phase.

With a spark plug, this phase is also divided in three phases: the breakdown phase with the creation of a plasma, the arc phase and the glow phase. At the end of the discharge, combustion will eventually start. During the ignition, temperatures in the plasma can reach 50 000K. At such temperature, important chemical effects such as dissociations and recombinations have to be accounted for.

To study these effects, a suitable chemical kinetic scheme should be used to account for both combustion and plasma chemistries. Some detailed mechanisms of both chemistries are available but are too costly for a DNS. A solution is to use an Analytically Reduced Chemistry (ARC) of both chemistries. An ARC reduces a detailed chemical mechanism to a mechanism containing less species and reactions which make this new mechanism affordable for a DNS.

The aim of this work paper is to study the effect of the plasma chemical kinetics on the ignition process. To do so, four 3D DNS are performed. Those simulations are using the academic anode-cathode configuration with the AVBP solver. Two simulations are performed: with an ARC coupling combustion and plasma kinetics for a first discharge in pure air and a second in an air/propane mixture of $\phi = 1$.

In the first part of this report, a presentation of the study is made with a description of the project, a literature review of ignition and a review of previous studies made at CERFACS in the frame of the FAMAC project. Then, the second part presents the numerical tools used for this study via the presentation of the solver AVBP and the description of all used numerical models. Finally, the third part is dedicated to the DNS of the ignition of the anode-cathode configuration with the presentation of the configuration and numerical investigations. Results are confronted to experimental data and a study of the chemical kinetic of the two first microseconds of the ignition is made.

5   Presentation of the study

5.1   Host Enterprise : CERFACS

CERFACS stands for "European Center for Research and Advanced Training in Scientific Computation"[1]. This research center is private and supported by seven shareholders being industry or public institutions: Meteo-France, CNES, EDF, Airbus, Safran, Total and ONERA. The main research areas at CERFACS are numerical simulation and algorithmic solutions for large scientific and technological problems, in the context of High Performance Computing (HPC). Applications cover a wide range of problems, from fundamental research to industrial systems. HPC capabilities are offered from indoor capacity with two computers, Nemo and Neptune, which provide an aggregate peak capacity of 333 Tflop/s for processing. Then, outdoor capacities are also available such as computers from the CNES, the CEA or Idris.

There are five research groups at CERFACS:

- Computational Fluid Dynamics (CFD)

- Climate modelling and global change (GLOBC)

- Aviation and Environment

- Parallel algorithms

- IT management and user support

These groups are composed from interdisciplinary teams, both for research and advanced training that are comprised of physicists, applied mathematicians, numerical analysts, and software engineers. Within these teams several codes and tools are constantly being developed. The current study is performed in the CFD team, using the AVBP code for reacting turbulent flows developed by CERFACS and IFPEN[2].

5.2   FAMAC Project Description

This study is part of the ANR project started in 2012, called FAMAC for Fondamentaux d'Allumage pour Moteurs à Allumage Commandé, gathering various institutions such as CORIA, EM2C, LAPLACE, research companies such as CERFACS or IFPEN and one industrial partner: CONTINENTAL. The objective of the project is to better understand the early stages of spark ignition in order to offer innovative solutions for better performances.

The study of ignition systems for internal combustion engines has a great importance for the design and development of new engines. A constant design concern, always present in new developments, is the difficulty to ignite in an economic (i.e. with minimum energy) and reliable way. In addition, new engines will need to extend their operation limits to reach the future regulations on fuel consumption and pollutant emissions, which will make ignition even more difficult to achieve and control. As an example, European regulations on CO_2 emissions for road transportation vehicles state that by 2021 the fleet average to be achieved by all new cars is 95 grams of CO_2 per kilometer, reducing 35 grams of CO_2 per kilometer from the current regulation [1].

5.3   Literature review of ignition

5.3.1   From the electric discharge to the flame

In internal combustion engines, several ignition systems are found, like spark plugs, glow-plugs or even lasers for academic cases. The present project focuses only on spark plugs, where an electric discharge is delivered in the combustion chamber in order to ignite the fuel/air mixture.

---

[1] Centre Européen de Recherche et de Formation Avanée en Calcul Scientifique

[2] Institut Français de Pétrole Energies Nouvelles

According to a multitude of authors [2, 3, 4], with a spark plug, the ignition is divided in three phases: the breakdown phase, the arc phase and the glow phase as shown in Fig. 1. The arc phase is the intermediate phase between the breakdown and the glow, and is not represented on the scheme. At the end of the discharge, combustion will eventually start.

As described in Fig. 1, during the ignition process, a plasma is created. A plasma is a ionized gas consisting of positive ions and free electrons in proportions resulting in more or less no overall electric charge, typically at low pressures (as in the upper atmosphere and in fluorescent lamps) or at very high temperatures (as in stars and nuclear fusion reactors). In this study, we are interested in the second case, which is the plasma at high temperature.
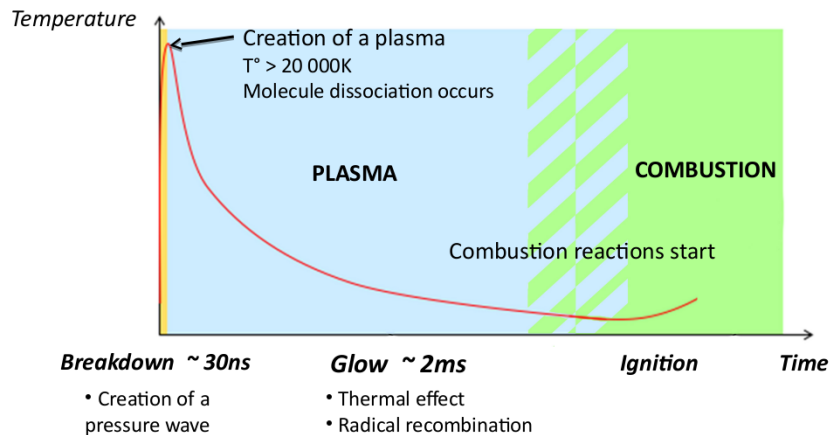

Figure 1: Sketch of the evolution of temperature during the first instants of ignition

First of all, the ignition starts with the breakdown (~1-10ns) via a big amount of energy in order to reach the activation energy of reactions for the creation of radicals. At this time, a cylindrical plasma channel develops with a brutal temperature rise to 60 000K [2] and the emission of an intense shock wave. The gas molecules inside the channel are fully dissociated and ionized. This energy supplied is transferred via dissociation and ionization almost without loss to the plasma.

Then, the arc phase(~1μs) with an increase of pressure and of the volume of the plasma channel. Thus, the temperature drops as a function of time around 8000K and part of the potential energy (dissociation and ionization) is reconverted to thermal energy. During this phase, inside the plasma, temperatures are too high for stable particles. However, relatively low temperatures at the border of the channel combined with the presence of radicals lead to the first combustion reactions and to the flame kernel.

During the glow phase (~1ms), the temperature in the plasma decreases to around 3000K. The major part of electrical energy of the ignition system is transmitted during this final phase that lasts around a millisecond. All these steps contribute to succeed the ignition, the energy deposition has to be longer than the characteristic time of reaction to help the flame to propagate by itself. This can also be seen in terms of energy: the flame will extinguish if the energy delivered by the kernel is not big enough to overcome heat losses due to thermal diffusion.

Table 1 [2] presents the energy losses during each phase of the ignition process. The major part of the ignition energy comes from the glow phase. But the energy which creates the plasma comes from the breakdown phase because of its small duration and because of the small volume in which it occurs. Moreover, the losses of the breakdown by conduction to the electrodes is less than 6%.

Total energy loss	Breakdown 3%	Arc 3%	Glow 94%
Radiative loss	$< 1\%$	$\approx 5\%$	$< 1\%$
Conduction loss to the electrodes	$\approx 5\%$	$\approx 45\%$	$\approx 70\%$
Part of total energy used for the ignition	$\approx 3\%$	$\approx 1.5\%$	$\approx 28\%$

Table 1: Amount of energy loss and used for ignition for each phase of the ignition

Moreover, the energy of the arc phase is small compared to the energy delivered during the glow phase and is twice lower than during the breakdown.

Finally, as said previously, the major part of the energy comes from the glow phase delivered by the spark plug even with important losses by conduction to the electrodes.

5.3.2 The plasma chemistry

Because of unusual conditions of temperatures during the ignition, and specially during the breakdown phase, the composition of air differs from its composition at 300K as presented in the Fig. 2 showing the mixture composition of a plasma versus its temperature for an initial mixture composition of 79% nitrogen and 21% oxygen [5]. For the left figure, the volume remains constant in order to represent the mixture composition during the first phase of the breakdown when the breakdown energy is introduced during a very short time ($<1\mu s$) in a very small volume. And for the right figure, the pressure is constant in order to represent the plasma during its expansion which means during the glow phase.
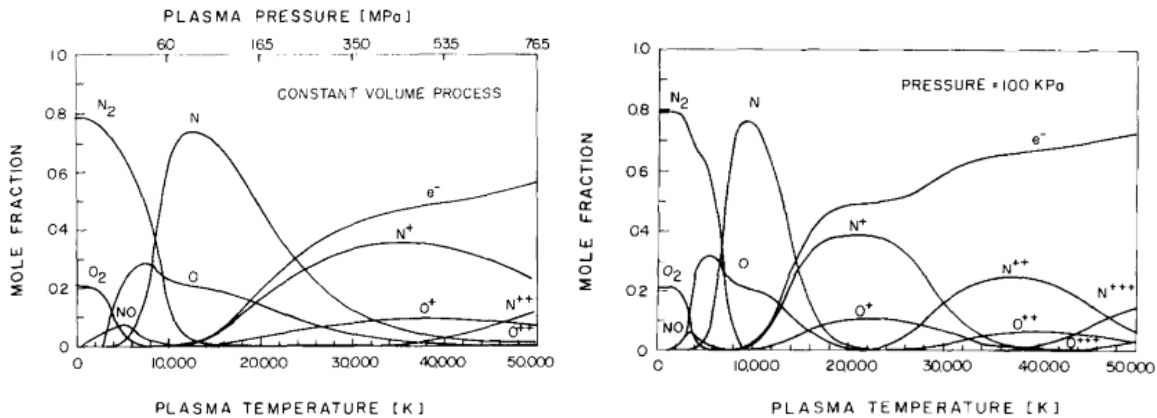

Figure 2: Mixture composition as a function of the temperature of an initial air mixture at 300K and 1bar at constant volume (left) and constant pressure (right).

At constant volume, O_2 and N_2 start to dissociate around 2500K and 5000K respectively. Both are fully dissociated over 14 000K and O and N begin to lose their electrons to become O^+ or N^+. At 40 000K, a second ionization occurs with N^{++} and O^{++}. At 50 000K, electrons represent almost 70% of the plasma composition.

On the other hand, at fixed pressure, the gas molecules are fully dissociated at 9000K and exclusively composed of ionized atoms and free electrons at 14 000K. The second ionization occurs at 35 000K. A third occurs over 50 000K.

At such temperatures, chemical effects are important to take into account and will be presented further.

5.4 Aim of the study and review of precedent works made in the FAMAC context

The aim of this work is to study the kernel formation following the electric discharge at the spark plug. Because of the different steps occurring during the ignition process, four physics have been studied.

First, with the brutal temperature rise, a thermal aspect. Then, dissociation in and at the border of the plasma and radical's creation, brings a kinetic chemistry aspect[6]. Moreover, the pressure rise leads to a shock which leads to a mechanical aspect [7]. Finally, the ionized plasma channel can lead to a magnetic/-electric phenomenon [8].

Each case has been studied separately and for each one some numerical validations have been made.

5.4.1 Review of the temperature's extrapolation behavior for thermodynamic and transport properties

Initially, with the code AVBP used by the CERFACS, a temperature higher than 5000K can not be reached which is enough for classical combustion phenomena. In order to take into account high temperatures and pressures reached in the plasma, Beceril [6] extended thermodynamics and transport properties to high temperatures. Thermodynamic properties have been extended by using as reference the NASA-9-coefficient polynomials [9]. Transport properties have been adapted by modifying the dynamic viscosity and the thermal conductivity using polynomial expressions given by d'Angola et al [10].

Those modifications have been validated using DNS [3] of a 1D premixed laminar and stationary CH_4/air flame of fuel-air ratio $\phi = 0.8$. For the kinetic part, a simplified chemistry with two reactions has been used (CM2 kinetic scheme [11]) :

$$CH_4 + 1.5O_2 \Rightarrow CO + 2H_2O$$

$$CO + 0.5O_2 \Leftrightarrow CO_2$$
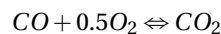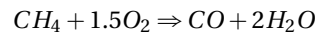
5.4.2 Review of the ignition's kinetic

During ignition, complex chemical mechanism occur and it is necessary to take them into account. In order to observe these chemical effects via dissociation, recombination and principal species in different zones of the ignition -the plasma channel, the shock wave and the combustion area-, two kinetics schemes have been used:

- CM2: a reduced scheme [11]

- The analytic scheme of Lu [12, 13, 14](73 reactions and 13 species)

Comparing these two chemical schemes allows to evaluate the importance of taking into account combustion radicals and a high number of elementary reactions.

Results and the analysis of Lu's scheme are given in the appendix 11.1. The complementary contribution of the analytic kinetic is the apparition of radicals of combustion.

5.4.3 Review of shock waves effects on the ignition

Additionally, Maestro [7] performed a full 3D ignition simulation with a real electrode geometry [15]. In terms of pressure wave or flame front, a good agreement was found between the AVBP simulation, the numerical results of Kravchik *et al.* [15] and the experimental results from Maly *et al.* [16] as shown in Fig. 3.

A comparison of the relative pressure between Kravchik's results and a simulation made with AVBP is also available in appendix 11.2 and shows a good agreement.

5.4.4 Review of the magnetic/electric effects on the ignition

The objective of this study was to evaluate the impact of magnetic/electric field on the ignition process after the spark discharge. To do so, results from a FLUENT plasma model (MHD) [4] were compared to AVBP simulations of both non reactive and reactive flows without the magnetic/electric fields. AVBP and FLUENT simulations correspond to an academic spark plug configuration from CORIA laboratory. The experimental

---

[3] Direct Numerical Simulation

[4] Magneto-hydrodynamics, combination of the Navier-Stokes equations of fluid dynamics and Maxwell's equations of electromagnetism
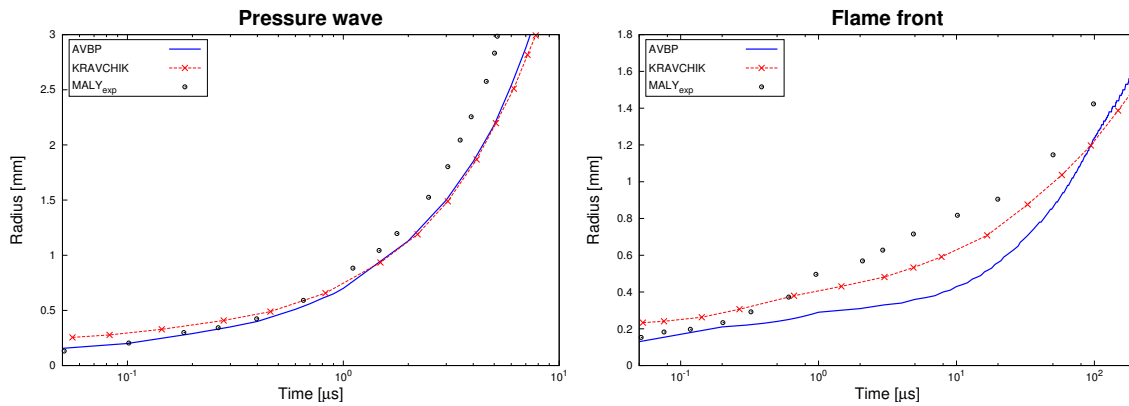
Figure 3: Temporal evolution of the location of the pressure wave and of the flame front for Maly experimentation, AVBP simulation and Kravchik calculations

results were obtained after a nanosecond pulse in air. Pressure and temperature probes data as well as Schlieren photographs are used to confront AVBP and FLUENT simulations.

No differences were observed with or without the magnetic/electric field, confirming its minor impact on the ignition process.

6 Numerical tools

The tools and models used in this study are described in this section.

6.1 Presentation of AVBP

Developed by the CERFACS and IFPEN, the AVBP code is a parallel CFD[5] unstructured solver. It is capable of handling grids of any cell type in order to solve the three-dimensional compressible, reactive conservation Navier-Stokes equations. It is used to perform DNS [6] and LES [7].

It can be applied to combustion chambers, turbo machinery, safety analysis, optimization of combustors or pollutant formation (CO, NO, soot). AVBP is used by multiple laboratories (IMFT, EM2C, TU Munich or Von Karmann Institute) and companies (SNECMA, TURBOMECA or Airbus Safran Launchers).

6.2 Standard set of equations for DNS

For this study, the DNS method is used.

A DNS is a simulation solving the complete set of compressible Navier-Stokes equations, without any type of model for the turbulence. It means to resolve all the scales of turbulence until the Kolmogorov's scale. Consequently, DNS is a really accurate and expensive simulation, suitable for small computational domains and academic cases. For the present study, DNS is a good candidate because of the small computational domain.

The set of conservative equations to solve reacting flows are presented here as in [17]. The index notation is adopted. Note however that the index k refers to the kth species and will not follow the summation rule unless specifically mentioned.

$$\frac{\partial \rho}{\partial t} + \frac{\partial \rho u_i}{\partial x_i} = 0 \tag{1}$$

$$\frac{\partial \rho_k}{\partial t} + \frac{\partial}{\partial x_j}(\rho_k u_j) = -\frac{\partial}{\partial x_j}[J_{j,k}] + \dot{\omega}_k \tag{2}$$

$$\frac{\partial}{\partial t}\rho u_j + \frac{\partial}{\partial x_i}\rho u_i u_j = -\frac{\partial p}{\partial x_j} + \frac{\partial \tau_{ij}}{\partial x_i} \tag{3}$$

$$\frac{\partial \rho E}{\partial t} + \frac{\partial}{\partial x_i}\rho u_i E = \dot{\omega}_T - \frac{\partial q_i}{\partial x_i} + \frac{\partial}{\partial x_j}(\sigma_{ij} u_i) + \dot{Q} \tag{4}$$

Equations [1- 4], are mass, species, momentum and energy conservation equations respectively where:

- ρ : density

- u_i : velocity vector

- E : total energy

- Y_k : mass fraction per unit mass of species k for $k = 1$ to $N-1$

- N : number of species

- $V_{k,i}$: diffusion velocity of species k

- $\dot{\omega}_k$: reaction rate of species k

- p : pressure

---

[5] Computational Fluid Dynamics
[6] Direct numerical simulations
[7] Large eddy simulation

- $\tau_{ij} = 2\mu(S_{ij} - \frac{1}{3}\delta_{ij}S_{ll})$: viscous tensor where $S_{ij} = \frac{1}{2}\left(\frac{\partial u_j}{\partial x_i} + \frac{\partial u_i}{\partial x_j}\right)$

- $\dot{\omega}_T$: heat release due to combustion

- $\dot{Q}$: external heat source term

- $J_{j,k}$: species diffusion flux

6.3   Numerical models used for ignition simulations

For the study, different numerical models were required in order to simulate the ignition:

- The combustion chemistry

- The plasma chemistry

- Thermodynamic and transport properties

- The energy deposition model

6.3.1   Analytical reduced chemistry (ARC) for combustion

Combustion reactions occur at the end of the ignition and a chemistry model is developed to simulate it. This part of the work has been made by Felix Collin-Bastiani [18] and has been integrated to this report to fully understand the path to the simulation.

Analytical reduced chemistry is a method which allows to reduce complex chemistries by reducing the number of reactions and transported species using successively reduction techniques such as Directed Relation Graph (DRG) methods and Quasi-Steady State Approximations (QSSA). It allows to get a simplified mechanism containing fewer transported species.

For this current study, one ARC was made for the chemistry of combustion. It is dedicated to propane combustion without any plasma chemistry and is derived using the YARC reduction code[19]. The chosen detailed mechanism is the iso-octane LLNL mechanism made of 6 964 reactions and 874 species.

The final analytical reduced chemistry is made of 25 transported species, 292 reactions and 16 QSSA species, and is called ARC_Propane later.

6.3.2   Plasma chesmistry

As seen in section 5.3.2, a plasma is at high temperatures and chemical effects occurs in it. To simulate it, the set of plasma chemical reactions with associated rate coefficients [20] has been used, called Plasma_Chemistry hereafter. It is made of 38 species and 366 irreversible reactions and has already been used and validated for plasma studies and has been validated [20].

Then, the two kinetics models -Plasma_Chemistry and ARC_Propane- are merged in order to create a new kinetic model which allows to study both plasma and combustion. When reactions involved in both mechanisms are found, the reaction rate used in the ARC_Propane is kept arbitrarily as differences between reaction rates proposed by both schemes are very small. All 13 charged species of the Plasma_chemistry, known to be very reactive, are put in QSSA.

The resulting merged mechanism called Merged_Chemistry is made of 586 reactions, 30 species in QSSA and 33 transported species. Among the transported species, 12 are coming exclusively from the combustion part, 8 exclusively from the plasma contribution and 13 are common to both mechanisms. These 13 common species are essential as they bridge the gap between combustion and plasma chemistries.

The Merged_Chemistry has been validated:

- Under 3000K: by making a comparison to the detailed LLNL mechanism and ARC_Propane for both laminar unstrained premixed flame at 1 bar and 298K and auto-ignition time at 1 bar and $\phi = 1$. No difference is observed as expected because the plasma part is not active at such temperatures.

- For higher temperatures: A constant pressure reactor is simulated starting with a stoichiometric C_3H_8-air mixture at $T_{ini} = 300K$. Then, the final temperature is imposed at 10 000K and the final composition is compared to the equilibrium composition of the mixture given by the CEA code [21] at the same final temperature. The mean relative error is about 7% with a maximum relative discrepancy of 17% for the atomic carbon molar fraction, which is acceptable for the current study.

6.3.3 Thermodynamic and transport properties

As for the chemistry, thermodynamic and transport properties need to be adapted to high temperatures.

Since the work of Becerril of implementing thermodynamic and transport properties as seen in section 5.4.1, the NASA database is used. Nowadays, properties are available for the 63 species involved here up to 6000 K at least and 20 000 K for some species. Properties are extrapolated up to 20 000 K when missing.

Viscosity and thermal conductivity properties of the mixture are those derived for high temperature equilibrium air plasmas by D'Angola. Dissociations and recombinations occurring at high temperature are then taken into account in the transport properties temperature dependency, contrary to classical laws such as the Sutherland law.

6.3.4 Energy deposition model

Finally, the energy given by spark plugs needs to be simulate using an energy deposition model.

As seen in 5.3.1, the ignition is composed of the breakdown (1-10ns), the arc ($1\mu s$) and the glow ($1ms$) phases. Those three phases need to be modelled for the simulation.

To do so, these phases are modelled in space and in time. An energy deposition model is then created as a volumic source term Q which is added in the transport energy equation. This model allows to create the initial kernel.

6.3.4.1 Temporal shape

For this study, the temporal evolution of the energy deposition model is calibrated using available experimental data of spark sequences. The form of the electrical energy E_{elec} as function of time is reconstructed. The energy transmitted to the gas comes from the electrical energy. A standard efficiency coefficient is imposed to the electrical energy to obtain the actual transmitted energy E_{ign} to the mixture after losses.

Moreover, the energy is considered to be deposited in two phases: the breakdown phase and the end of the discharge gathering arc and glow. Further, the end of the discharge will be call glow hereafter for simplicity.

The breakdown phase is too short to obtain accurate experimental data but the amount of electrical energy provided during the breakdown E_{bd} can be estimated experimentally as well as its duration t_{bd}. Then, the simplest estimation of the electrical energy dE_s consumed during a small time dt is obtained by considering a constant electrical power:

$$dE_s(t) = E_{bd}\frac{dt}{t_{bd}} \tag{5}$$

As explained before, the energy used by the ignition is obtained considering an efficiency coefficient fixed from the literature, as described in Table 1, $\eta = 95\%$:

$$dE_{ign}(t) = \eta dE_s(t) \tag{6}$$

Concerning the glow phase, its duration t_{glow} is given experimentally as well as its electrical energy E_{glow}. Thus, the given electrical energy dE_s is reconstructed using the voltage and the current signal as functions of time, and it is observed that the electrical power decreases almost linearly. So by supposing that the electrical energy decreases linearly during the glow phase, we get the second phase of the deposition:

$$dE_s(t) = \frac{2E_{glow}dt}{t_{glow}^2}(t_{spark} - t) \tag{7}$$

As for the breakdown, during the glow there are losses to the electrodes by conduction. An efficiency coefficient ζ is used and we get for the second phase of the ignition:

$$dE_{ign}(t) = \zeta \, dE_s(t) \tag{8}$$

6.3.4.2 Spatial shape

Spatially, the volume of the energy deposition is approximated by a cylinder between two electrodes and an hyperbolic tangent function is used to smooth the deposition around this cylinder. A sketch of the spatial shape is presented in fig. 4:
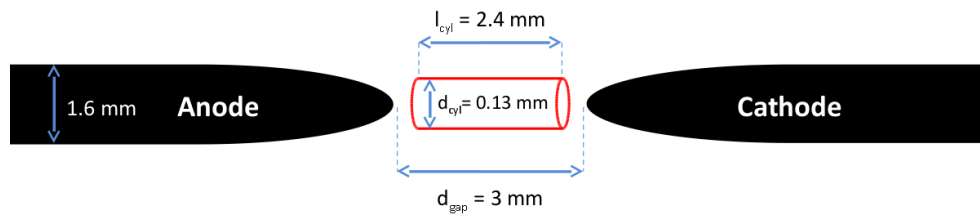

Figure 4: Sketch of the spatial shape of the energy deposition

7 Direct numerical simulations of the ignition

The simulation of the ignition with a DNS is presented in this part.

7.1 Configuration and numerical set-up

7.1.1 Configuration

For this study, an academic experimental configuration from CORIA laboratory is used. It is simply a pin-pin configuration, consisting of one cathode and one anode of $1.6mm$ maximum diameter and separated by $3mm$ as described in Fig. 4.

For the simulation, three symmetry hypothesis have been made. First, there are two symmetry planes from the revolution symmetry around pins. Second, for simplicity, we consider a symmetry plane between both electrode heads. Even if experimentally, a temperature gradient is observed between those electrodes during the spark.

Then, we get a numerical domain reduced to 1/8 of a sphere as presented in Fig. 5. The radius of this 1/8 of a sphere is about $10cm$ and its origin is at the left bottom corner.
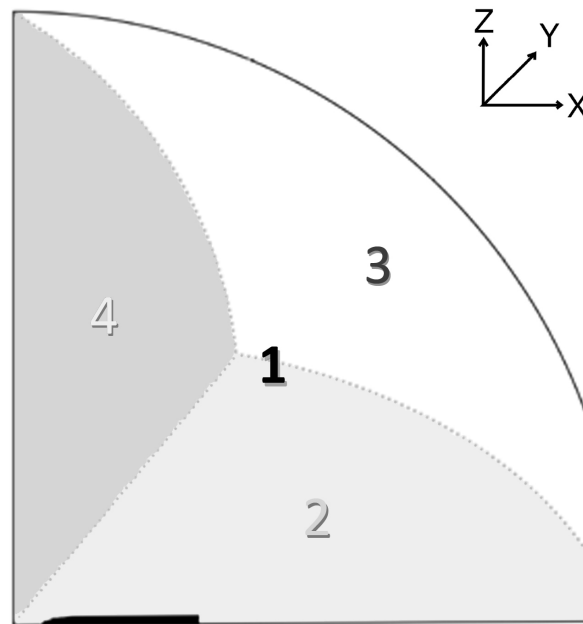
Figure 5: Sketch of the spatial shape of the deposition model

The head of the electrode is located at $[x = 1.5mm, y = 0.0mm, z = 0.0mm]$ to get a gap between the second dummy electrode of $3mm$. Symmetry planes are (xy,xz,yz). Symmetry conditions are then applied on faces 1, 2 and 4. For the face 3, a NSCBC condition [22] is used in order to fix the pressure to $1bar$. For the electrodes walls, a no-slip adiabatic condition is used because efficiency coefficients already account for conduction losses at the electrodes as explained in section 6.3.4.1.

7.1.2 Numerical set-up

During the breakdown, the energy is important in the inter-electrode gap, and strong gradients occur as well as chemical source terms. In order to be enough discretized, a 2.1 million tetrahedral cells mesh is used

with a characteristic grid size in the inter-electrode gap of 15 microns for the two first microseconds of the physical time.

After $2\mu s$, the breakdown is over and the temperatures is lower. The solution is then interpolated on a new mesh of 1.0 million cells with the smallest grid size in the inter-electrode gap of 50 microns.

For this simulation, the third-order explicit TTGC centered scheme is used. The time step is constrained by convection and diffusion processes via a CFL and a Fourier number and also by the chemical system. During the first $2\mu s$ of physical time, the time step ranges from $0.03ns$ to $0.5ns$. After $2\mu s$, it grows up to $1ns$. Finally, chemistry sub-cycling is also used for the first $2\mu s$ in order to improve the stability of the explicit time integration.

7.2 Numerical investigations

In this section, different studies of ignition are performed. First, a qualitative description of an ignition sequence is presented. Then, the influence of taking into account the plasma chemical kinetics or not is evaluated by looking at the temperature comparison of the hot gas kernel during the very first milliseconds after the discharge. Two cases are considered: pure air and propane-air mixtures. In a second step, numerical results are compared to experimental data and the influence of some ignition numerical parameters are assessed.

To do so, four cases are simulated at atmospheric conditions:

- A discharge in pure air to understand the impact of plasma reactions on the $O_2 - N_2$ mixture dynamics. This case is divided in two simulations:

  - The first one considering no chemical reaction and using a simplified model of the air with only N_2 et O_2 molecules in the mixture. All the energy is then used for thermal heating of the mixture
  - A second one considering the merged chemistry by using the Merged_Chemistry model

- A discharge in a propane-air mixture with $\phi = 1$, also divided in two simulations:

  - Considering only combustion reactions by using the ARC_Propane model
  - Considering the merged chemistry by using the Merged_Chemistry model

For the second discharge with propane, as for the pure air case, electrical signals from experiments are used to reconstruct the model inputs. The description of the amount of energy deposited for each ignition cases is described in Table 2.

Ignition cases	E_{bd}	t_{bd}	E_{glow}	t_{glow}	d_{cyl}	ef_{bd}	ef_{glow}
Pure air	$2.8mJ$	$20ns$	$77mJ$	$2.7ms$	$130\mu m$	0.6	0.25
Air with propane ($\phi = 1$)	$5.0mJ$	$20ns$	$110mJ$	$4.0ms$	$200\mu m$	0.6	0.25

Table 2: Amount of energy deposited for each ignition case

Because the numerical domain is a 1/8 of a sphere, energies indicated in this table are divided by 8 to get the real energy delivered in a 1/8 of a sphere. The breakdown time is fixed to $20ns$ because of the difficulty to measure it during experiments. Furthermore, the energy delivered for the propane-air ignition is higher than for the pure air ignition. The diameter of the energy deposition cylinder is the same for both simulations and is $130\mu m$.

Experimental data are available until $10ms$ isimulating such a long physical time is very costly. For three of the four simulations because of the complex chemistry used and the fine mesh. To get $10ms$ of physical time for the longest simulation, the simulation time is estimated to several weeks using 256 processors. Only the first configuration with no chemistry allows to get the first $10ms$ in less than a week and so to make several times for a parameter calibration, which is a good compromise for a 6 months work.

7.2.1 Qualitative description of the first instants of the ignition

Figures (6 & 7) show the simulation of a discharge in pure air without chemical reactions. Figure 6 presents temperature and pressure fields at four different moments of the beginning of the ignition before $2\mu s$. For each image, the upper part correspond to the temperature and the lower part to the pressure. Figure 7 presents only the temperature field at three different moments after the two first microseconds.

The two first instants of Fig. 6, at $40ns$ and $256ns$, give an idea of the expansion of the hot gas kernel at the beginning of the ignition. This expansion is controlled by a shock wave clearly visible at $804ns$ and $2\mu s$ by its front of pressure.
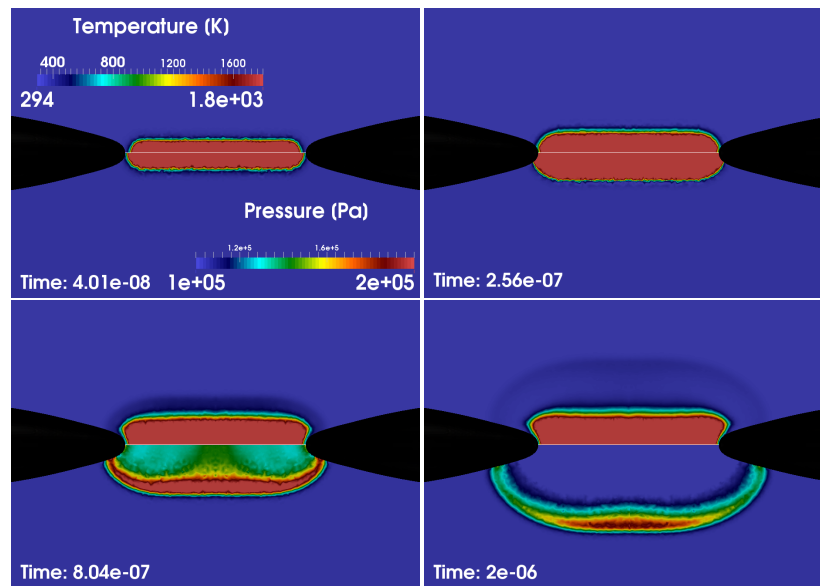
Figure 6: Temperature (top) and pressure (bottom) fields at four different moments of the two first micro seconds of the ignition for the simulation in pure air without chemical reactions

After $2\mu s$, inside the shock wave, the gas moves outwards with a high velocity. A depression is then observed between the two electrodes. This depression develops into a torus by leading the hot gas kernel to an inward gaseous flow near the spark gap and then to a pair of vortices with rotations in opposite directions as presented by Kono et al. [3]. This torus is presented in the Fig. 7 at $0.16ms$ around the hot kernel with a cooler area of temperature.

Then, this torus completely separates from the hot kernel and, by diffusion, slowly disappears. After the creation of the torus, the hot kernel will also expand by diffusion until the end of the glow phase. Figure 7 at $2.7ms$, which correspond to the end of the glow, presents the expansion of the hot kernel gases into a diamond shape. Afterwards, no energy is supplied so the hot kernel will cool down until equilibrium. The last image of Fig. 7 shows that the temperature considerably decreases and the hot kernel almost disappears (t=9.99ms).

The simulation represents qualiteviley well the different steps presented in the theory described in section 5.3.1.

7.2.2 Effects of the chemical kinetic during the first instants of the ignition process

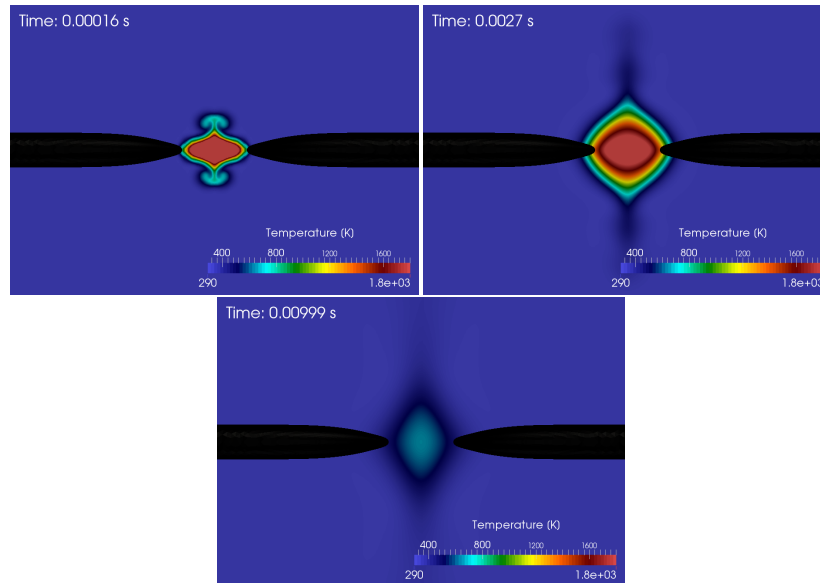In this part, the effects of the chemical kinetic is presented.

Figure 7: Temperature fields at three different moments of the ignition in pure air without chemical reactions

7.2.2.1 Temperature of the hot kernel gas

Before studying the composition of the mixture in the hot kernel gas, a first study of the influence of the chemistry on the temperature might give a first overview.
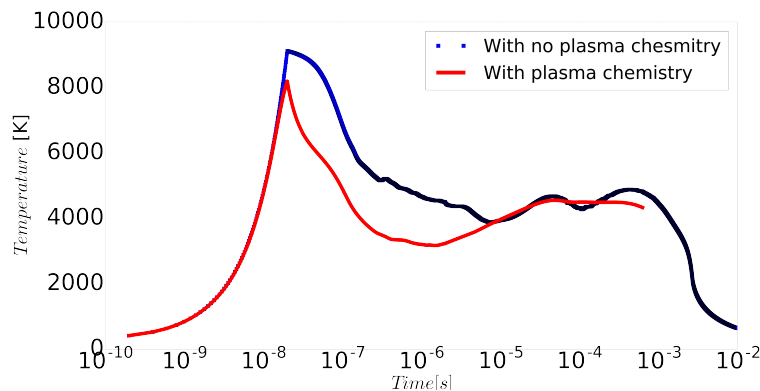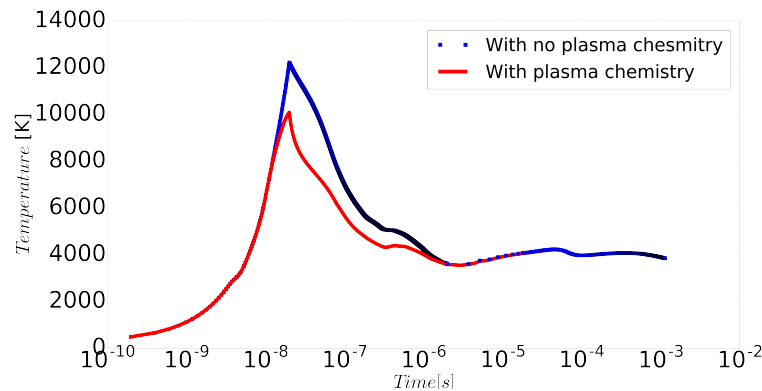

Figure 8: Temperature evolution versus time near the center of the hot gas kernel for a spark discharge in pure air with and without chemistry

Figure 8 compares the temporal evolution of the temperature near the center of the hot kernel gas with and without the plasma chemistry for a discharge in pure air. Until the end of the breakdown, around $20ns$, no difference is observed. After $20ns$, differences exist. Without any reaction, the temperature reaches 9000K at the end of the breakdown. With all plasma reactions, the maximum temperature reaches only 8000K at the end of the breakdown. This difference is due to the energy used by dissociation and ionization reactions, which are endothermic. For the case with no chemistry, all the energy given to the mixture is exclusively used for heating.

Thereafter, for the simulation with chemistry, the temperature first decreases before rising again because of exothermic recombination reactions occurring at lower temperatures.

For the simulation without chemistry, the temperature also increases because of the creation of the torus. Indeed, the creation of the torus moves the hot kernel hot gas into the center of itself which concentrates its energy into a lower volume. This leads to a higher temperature at the center of the hot kernel gas.

Then, after $2.7ms$, the temperature decreases drastically until equilibrium.

The temperature evolution for the discharge in a propane/air mixture is presented in Fig. 9. Similar results are obtained. The temperature for the case without plasma chemistry reaches higher levels than with a plasma chemistry. Then, the temperature decreases for both cases and is almost equal from approximately $2\mu s$. The simulation without the plasma chemistry still have the combustion chemistry for simulations with propane. So after approximately $2\mu s$, only combustion reactions seems to happen in the hot kernel gas.

Figure 9: Temperature evolution versus time near the center of the hot gas kernel for a spark discharge in a propane-air mixture ($\phi = 1$) with and without plasma chemistry.

Conversely, for the discharge in pure air, even after $2\mu s$, a difference appears with and without chemistry. Even if temperatures are similar, they are not equal. This difference is due to no reaction at all for one of the case and so only diffusion and convection phenomenons are taking into account. So the amount of energy leading by convection and diffusion are not the same because the chemistry is taking energy from the energy deposition model. Thus leads to a difference of temperature because the deposited energy is not exclusively used in convection or diffusion.

Eventually, the plasma chemistry seems to get a direct impact on the hot kernel temperature until approximately $2\mu s$. A study of its mixture composition is presented in following section.

7.2.2.2   Mixture composition of the hot kernel

To understand the difference of temperature observed with or without the plasma chemistry, a study of the plasma chemistry is necessary.

Figs. 12, 13 and 14 present mass fraction and production rates of O, O_2, N and N_2 at $10ns$, $20ns$, $100ns$ and $2\mu s$ versus the height at the center of the inter-electrode gap as presented in Fig. 10. For simulations with the complete chemistry, major reactions rates are also presented. For simulations with propane, reaction rates are similar and the only difference appears for reactions which are taking into account dinitrogen and nitrogen. Those reactions are not in the ARC_Propane model. So only reactions rates with the plasma chemistry are presented to avoid repetitions.
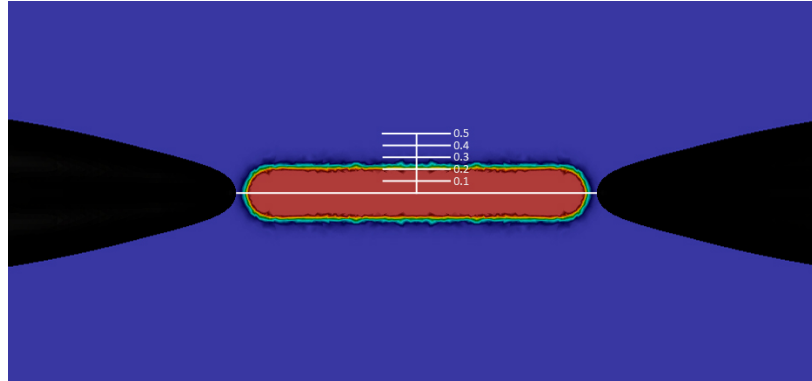
Figure 10: Sketch of the pin pin configuration with horizontal lines at 0.1, 0.2, 0.3, 0.4 and 0.5mm

Discharge in pure air   For the discharge in pure air as presented in Fig. 12, at $10ns$, O_2 and N_2 are not fully dissociated yet even if the temperature is around 5000K. But the dioxygen already start to dissociate to oxygen as presented with productions rates of O and O_2 which seems to be opposite. Moreover, major reactions which activate in the kernel at $10ns$ are:

$$O_2 + N_2 -> 2O + N_2 \tag{9}$$
$$2O_2 -> 2O + O_2 \tag{10}$$
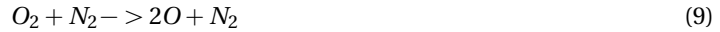
Those reactions rates validate the dissociation of the dioxygen to the oxygen at $10ns$.

Then, at $20ns$, the dioxygen is partially dissociated at the center of the kernel and the oxygen is partially created. Furthermore, the dinitrogen starts to dissociate into nitrogen. At this time, major reactions take into account mostly dioxygen and dinitrogen as reactants and nitrogen, nitric oxide (NO) and oxygen as product.

Later, at $100ns$, the temperature is around 5000K and the dioxygen is almost fully dissociated into oxygen. The dinitrogen is slightly dissociated but the temperature is not high enough to dissociate it totally. Furthermore, major reactions rates indicates that the dinitrogen already starts to recombine with the reaction:

$$N + NO -> N_2 + O \tag{11}$$

Finally, at $2\mu s$, the dinitrogen is almost fully recombined and recombinations of the dioxygen already started.

To conclude about the discharge in pure air, major dissociation (red) and recombination (blue) reactions of dioxygen and dinitrogen are:

$$\color{red} O_2 + N_2 -> 2O + N_2 \tag{12}$$
$$\color{red} 2O_2 -> 2O + O_2 \tag{13}$$
$$\color{red} O_2 + O -> 3O \tag{14}$$
$$\color{red} O_2 + N -> NO + O \tag{15}$$
$$\color{red} N_2 + O -> N + NO \tag{16}$$
$$\color{blue} N + NO -> N_2 + O \tag{17}$$
$$\color{blue} NO + O -> O_2 + N \tag{18}$$
$$\color{blue} NO^+ + N_2 -> N_2^+ + NO \tag{19}$$
$$\color{blue} N_2^+ + NO -> NO^+ + N_2 \tag{20}$$
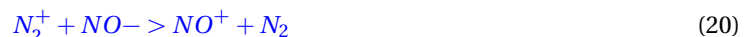
Fig. 11 presents a qualitative reaction scheme of the dissociation and recombination of O_2 and N_2 with O, N and NO versus time divided in four steps. Each reaction is represented with different color and the

indicated number corresponds to the number of the reaction. Dashed lines helps to remind that all species are not consumed in a reaction at each step. Only a part of a reactant is transformed into a product.
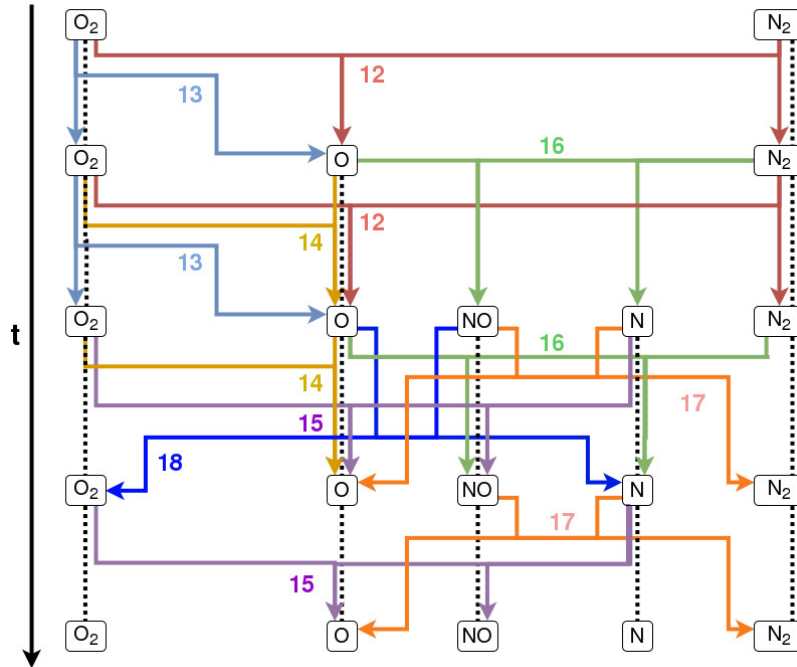
Figure 11: Qualitative reactional scheme of the dissociation and recombination of O_2 and N_2 with O, N and NO versus time

Initially, there is only O_2 and N_2 in the domain, so only reactions which have those molecules as reactants can start the dissociation. This scheme easily shows that the dissociation of the oxygen begins with two reactions: reaction 12 with only O_2 as reactant and reaction 13 with O_2 and N_2 as reactants. Those two reactions transform those reactants to O_2, N_2 and O. Then, the created oxygen reacts in a third reaction 14 to dissociate the O_2. The oxygen also reacts in reaction 16 to transform into NO and N. Finally, with the presence of nitrogen, reaction 15 transforms N and O_2 into O and NO.

Then, there are two recombination reactions: Reaction 18 transforms O and NO into O_2 and N and reaction 17 transforms N and NO into O and N_2.

Discharge in a propane/air mixture For the discharge in a propane/air mixture, results are similar to the discharge in pure air but because of an higher temperature, dissociations and recombinations are more important. Results are presented in Figs. 13 and 14.

At $10ns$, the temperature is higher than 6000K and the dioxygen has already started to dissociate into oxygen with or without plasma chemistry. For both simulations, the dinitrogen has started its dissociation. With the plasma chemistry simulation, major reactions are the dissociation of the dioxygen into oxygen or OH and HCO:

$$H + O_2 -> O + OH \tag{21}$$

$$CH + O_2 -> HCO + O \tag{22}$$

At $20ns$, the temperature reaches 10 000K for both simulations. For both, the dioxygen has considerably been dissociated into O. The dinitrogen started to dissociate into N only with the plasma chemistry. Without plasma chemistry, the dinitrogen remains constant. At $20ns$, there are two major reactions with their

backward reactions:

$$H + O_2 <-> O + OH \tag{23}$$

$$N_2 + O <-> N + NO \tag{24}$$

At this time, the forward reaction of 24 is more than two times more active than its backward reaction. Dissociations of N_2 are then predominant at $20 ns$. The forward and backward reaction rates of 23 are similar and both reactions almost cancel each other.

At $100 ns$, the temperature is around 6000K for both simulations and the dioxygen is totally dissociated with the plasma chemistry.

Finally, at $2 \mu s$, the temperature is around 4000K for both cases and the dinitrogen is fully recombined with the plasma chemistry. On the other hand, the dioxygen is partially dissociated and is recombined with and without the plasma chemistry. TThere is one major reaction with its backward reaction, which cancel each other by producing and consuming H, O_2, O and OH:

$$H + O_2 <-> O + OH \tag{25}$$

For the discharge in a propane/air mixture, major dissociation and recombination reactions of the dioxygen and of the dinitrogen are:

$$H + O_2 -> O + OH \tag{26}$$

$$O + OH -> H + O_2 \tag{27}$$

$$N_2 + O -> N + NO \tag{28}$$

$$N + NO -> N_2 + O \tag{29}$$

$$CH + O_2 -> HCO + O \tag{30}$$

The mechanism is similar to the discharge in pure air. Differences comes from the presence of the propane, i.e. carbon and hydrogen atoms. The dissociation of the dioxygen begins at a lower temperature with reactions 26 and 30. Those reactions create oxygen and OH and both are used in the following step via reactions 27 and 28 to produce NO and some nitrogen. Then, a third step uses the transformed nitrogen for the recombination to the dinitrogen with the reaction 29.

To conclude, this part of the study shows the influence of the plasma chemistry on the two first microseconds of the ignition process. The difference of temperature is mainly due to dissociations and recombinations of dinitrogen and dioxygen in the hot kernel. From propane/air simulations, it seems that this difference is mostly due to dissociations and recombinations of the dinitrogen because dissociation reactions of the dioxygen exists in the combustion chemistry.
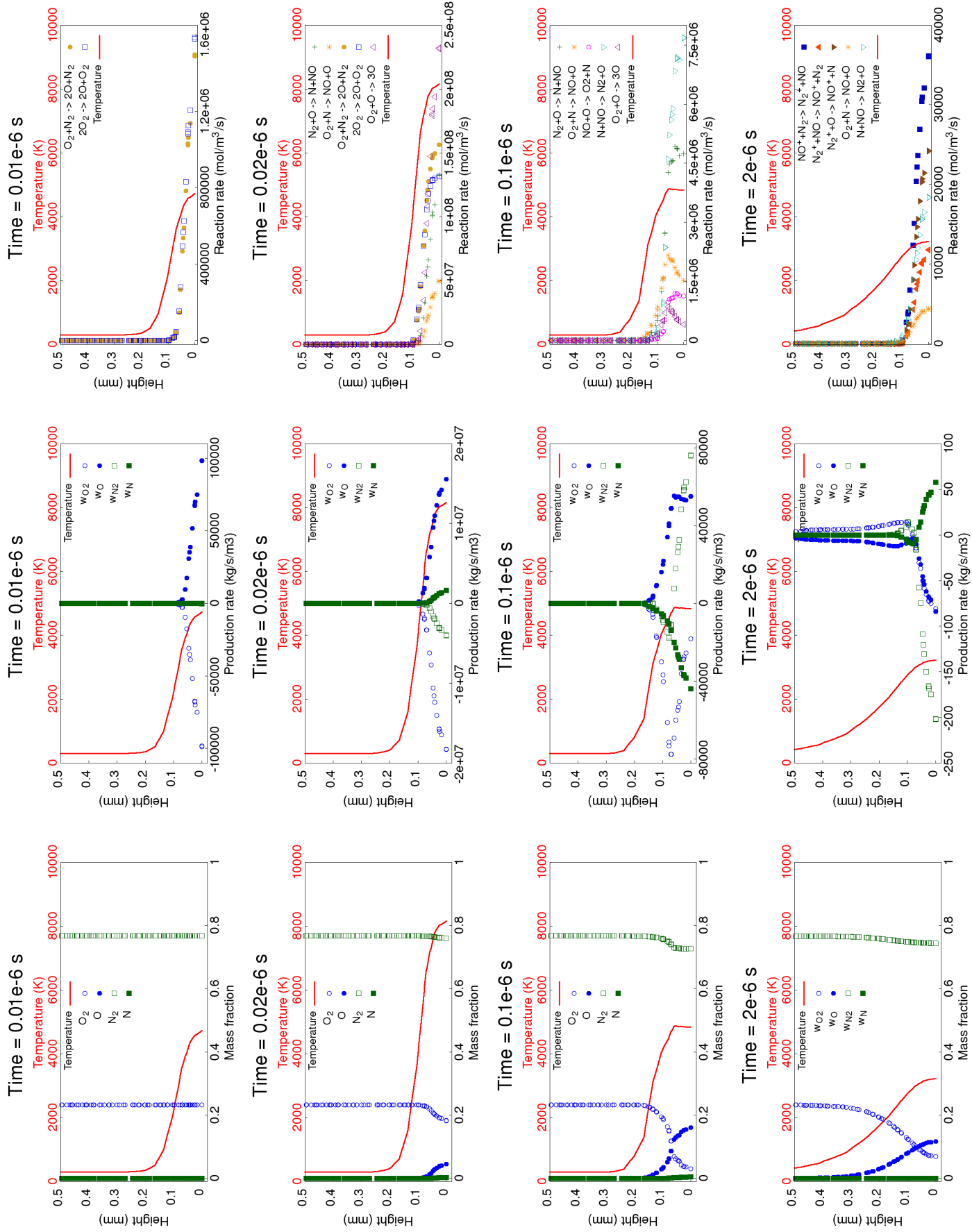
Figure 12: Mass fractions and production rates for O, O_2, N and N_2 and major reaction rates at $10ns$, $20ns$, $100ns$ and $2\mu s$ for a discharge in pure air with chemistry
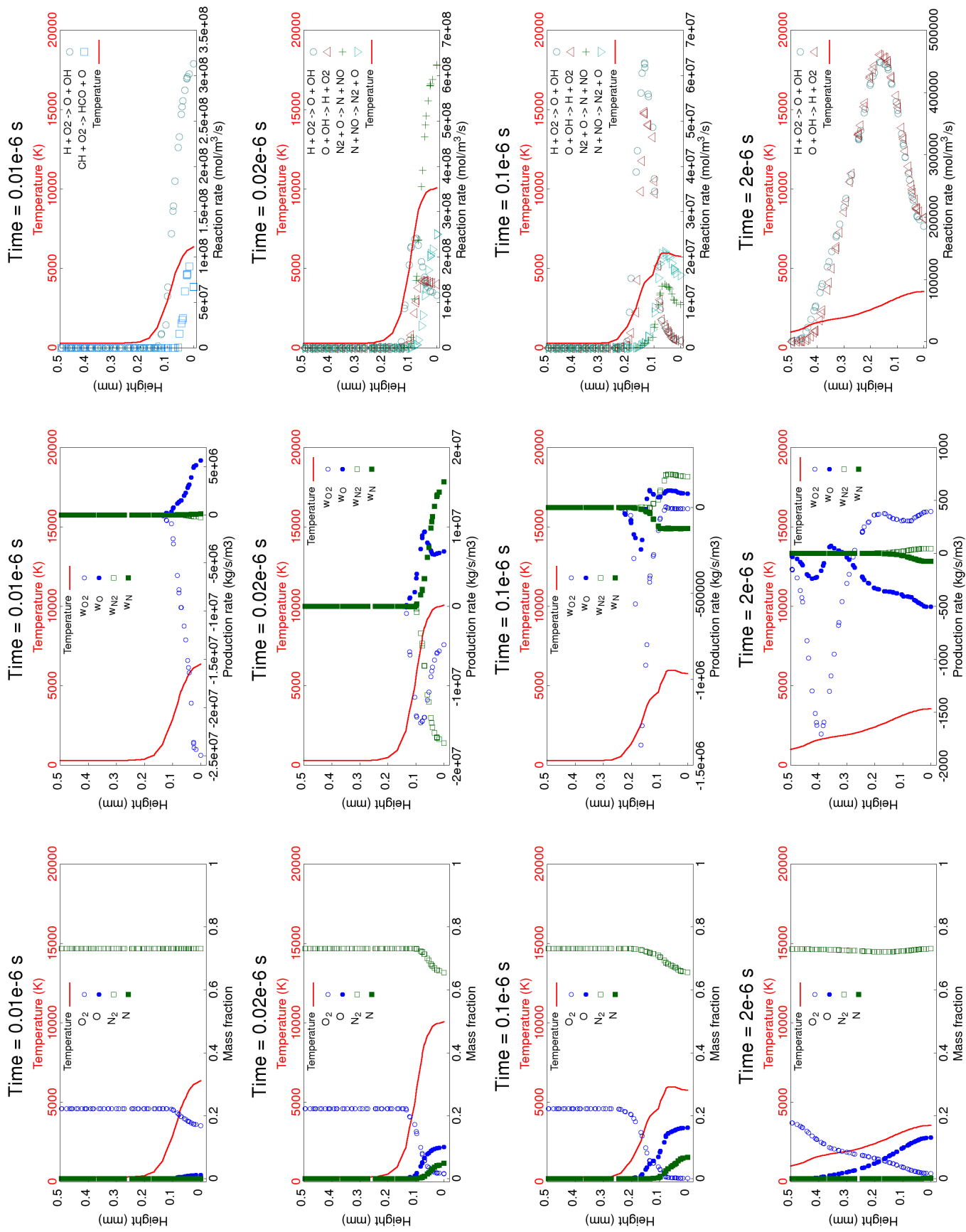
Figure 13: Mass fractions and production rates for O, O_2, N and N_2 and major reaction rates at $10ns$, $20ns$, $100ns$ and $2\mu s$ for a discharge in a propane/air mixture with plasma chemistry
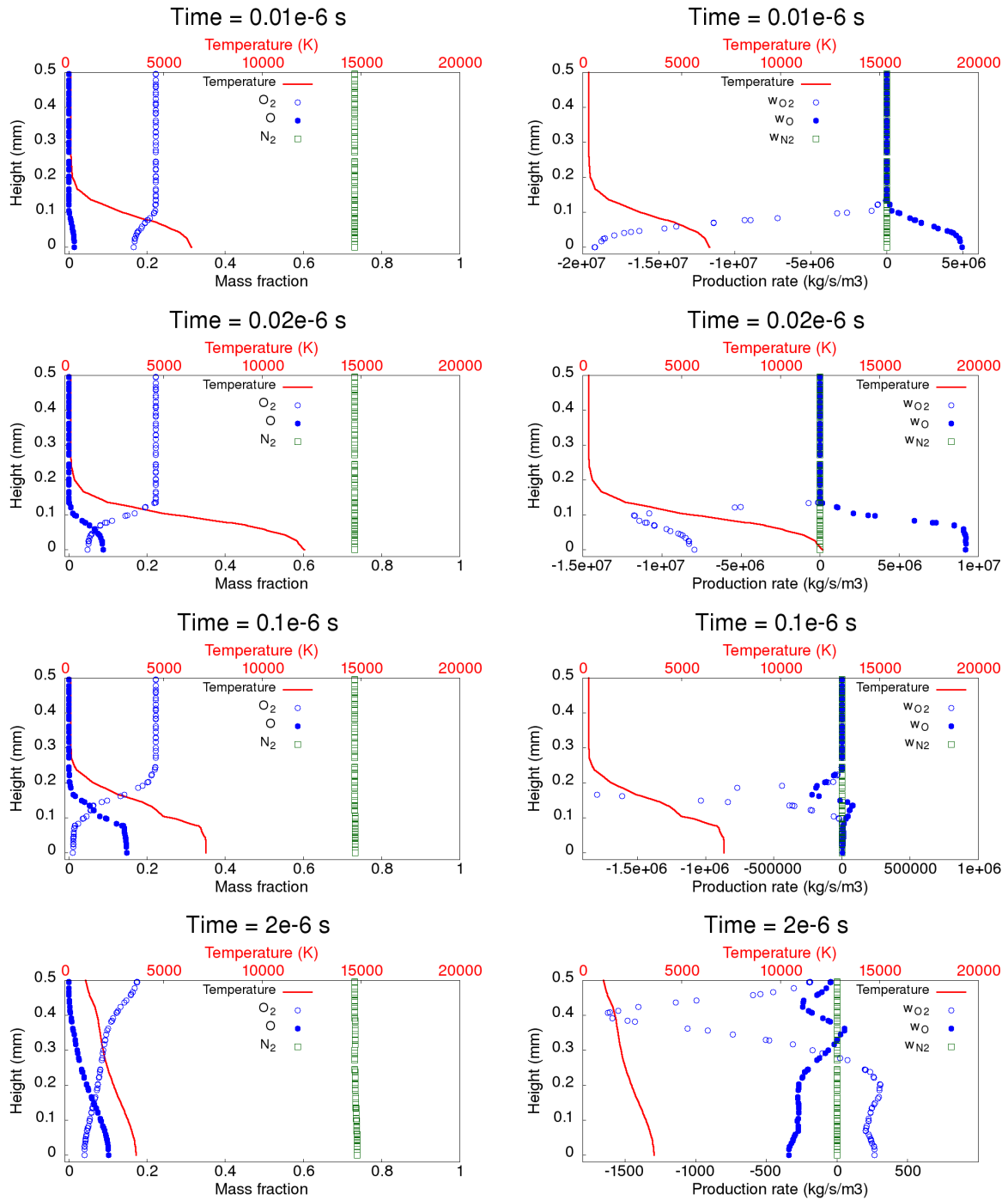
Figure 14: Mass fractions and production rates for O, O_2, N and N_2 and major reaction rates at $10ns$, $20ns$, $100ns$ and $2\mu s$ for a discharge in a propane/air mixture without plasma chemistry

7.2.3 Comparison of numerical simulations to experimental data and effect of the glow and breakdown phases on the ignition process

This part has two goals. First to validate the simulation by comparing it to experimental data. Second to study the effect of the glow and breakdown energies on the ignition. To fully understand the following figures, Fig. 15 presents different coordinates of heights and width in the domain.
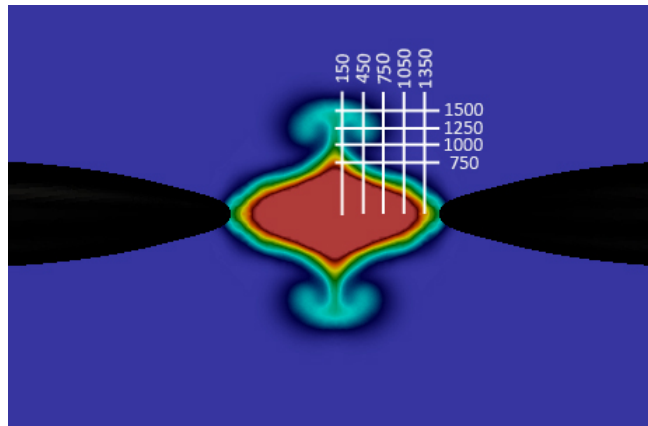
Figure 15: Sketch of the pin pin configuration with coordinates in micrometers of different points at different widths(x) and heights(y)

7.2.3.1 Comparison of numerical simulations to experimental data

The reference simulation is Ef_{bd} = 0.6 & Ef_{glow} = 0.25 as presented in Table 2 which corresponds to blue lines or blue points in Figs. 16, 17 and 18. Those reference parameters have been choosen after several calibration simulations.

Figure 16 is a comparison to experimental data of the temperature evolution versus time at different points of the domain and for three simulations. Figure 17 is a comparison to experimental data of the reference simulation at $5ms$ and $10ms$. And the Fig. 18 is a comparison to experimental data of the temperature at different heights versus the width of three different simulations.

First of all, on Fig. 16, experimental data presents two phases with two peaks of temperature. The first peak corresponds to the breakdown which happens around $20\mu s$ and reaches $1000K$. Then, the temperature decreases and a second peak of temperature at $2500K$ is visible around the millisecond which corresponds to the glow phase. Then, the temperature drastically decreases because of the end of the glow.

Such results with two peaks of temperature are also visible in the simulation but the peaks arrive too early. In terms of maximum temperature, simulation and experiment are similar. Those results are confirmed with the Fig. 18. Temperatures at $500\mu s$ and $750\mu s$ are too high for the experiment. Then, at $1200\mu s$ there is not much differences but this is a coincidence because at $2000\mu s$, the simulation is too cold and a difference of more than 500K is presented in the center at $750\mu m$.

Eventually, temperatures are too high at the beginning of the ignition and then are too low. This might be due to the value of the diameter of the cylinder, where the energy is deposited. Moreover, at $1200\mu s$ and $750\mu m$, experimental data present an asymmetrical shape as well as at other times and other heights. Since the developed model uses a symmetry hypothesis of the energy deposition delivered between the anode and the cathode, this hypothesis needs to be modified.

Experimentally, there is no measurement of the dimension of the plasma created during the discharge. Knowing the volume or the shape of the plasma is important for the numerical simulation. In order to retrieve the experiment with simulations, some parameters need to be calibrated such as the energy deposition shape or its diameter by adjusting the efficiency of the breakdown and glow energies transfer.
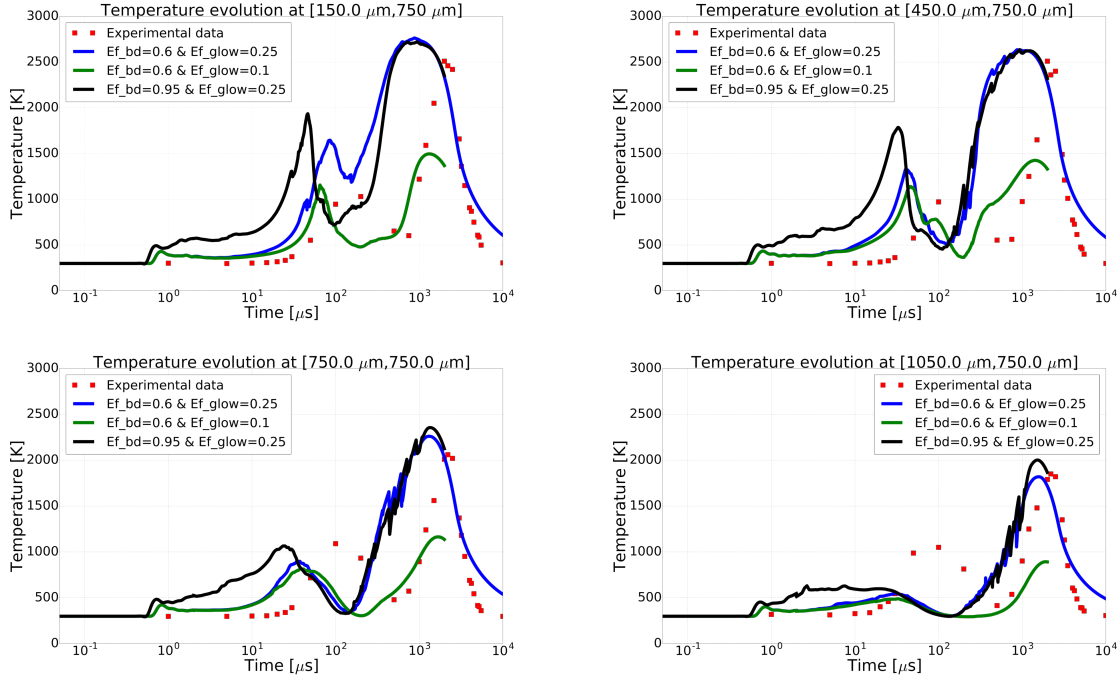
Figure 16: Comparison with experimental data of three different temperature evolutions versus time at different locations ($[150\mu m;750\mu m]$, $[450\mu m;750\mu m]$, $[750\mu m;750\mu m]$, $[1050\mu m;750\mu m]$)

7.2.3.2   Impact of the glow and breakdown on the ignition

In order to study the impact of the energy transfer efficiency on the ignition, some parameters are modified. The reference simulation is the same as for the comparison to experimental data. For the study of the energy transfer efficiency during the glow phase, the glow efficiency is lowered because $Ef_{glow} = 0.25$ is already a theoretical high value. Conversely, for the energy transfer efficiency during the breakdown phase, the breakdown efficiency is increased because $Ef_{bd} = 0.6$ is theoretically a low value. Parameters of the three simulations are described in the Table 3 with Ef_{bd} the breakdown efficiency and Ef_{glow} the glow efficiency.

Name of the simulation	E_{bd}	Ef_{glow}
Ref	0.6	0.25
Low_Glow	0.6	0.1
High_Bkd	0.95	0.25

Table 3: Parameters of the three simulations to study the impact of the glow and breakdown phase

Impact of the energy transfer efficiency of the breakdown phase on ignition   In this part, only the Fig. 16 is relevant to understand the impact of the breakdown on the ignition. For every width, High_Bkd presents higher temperature than Ref. And all peaks of temperature are earlier for the High_Bkd than for Ref.

At the point $[150\mu m;750\mu m]$, with a strong breakdown efficiency, the peak of temperature happens around $50\mu s$ for almost $2000K$ and with a low breakdown efficiency, this peak is around $100\mu s$ for $1700K$.
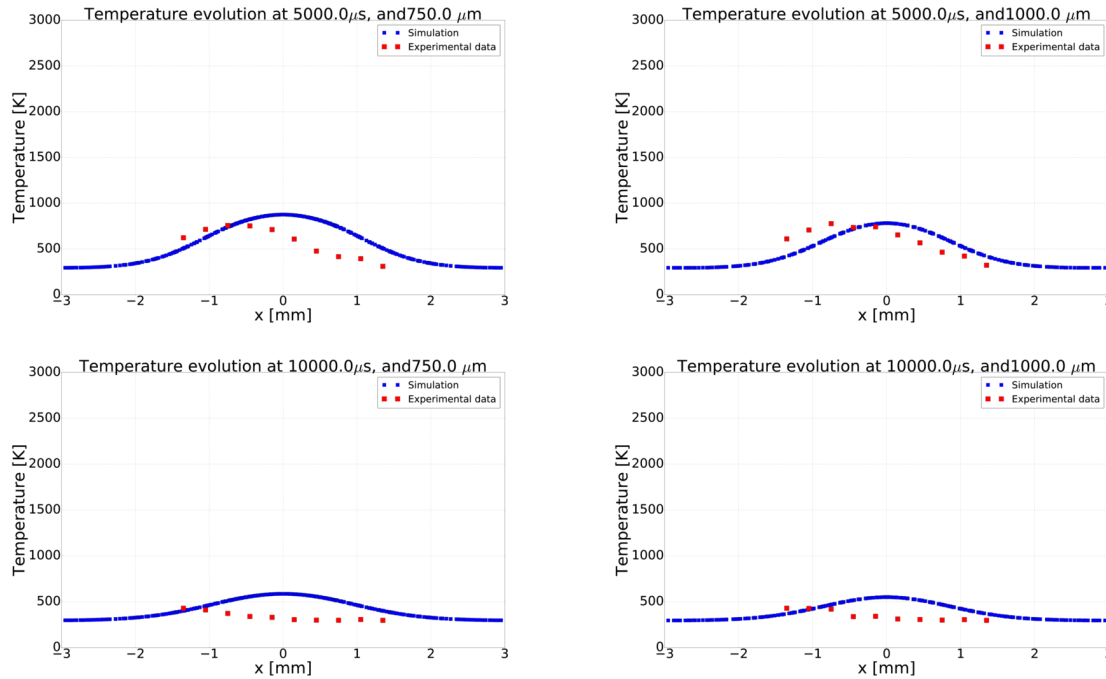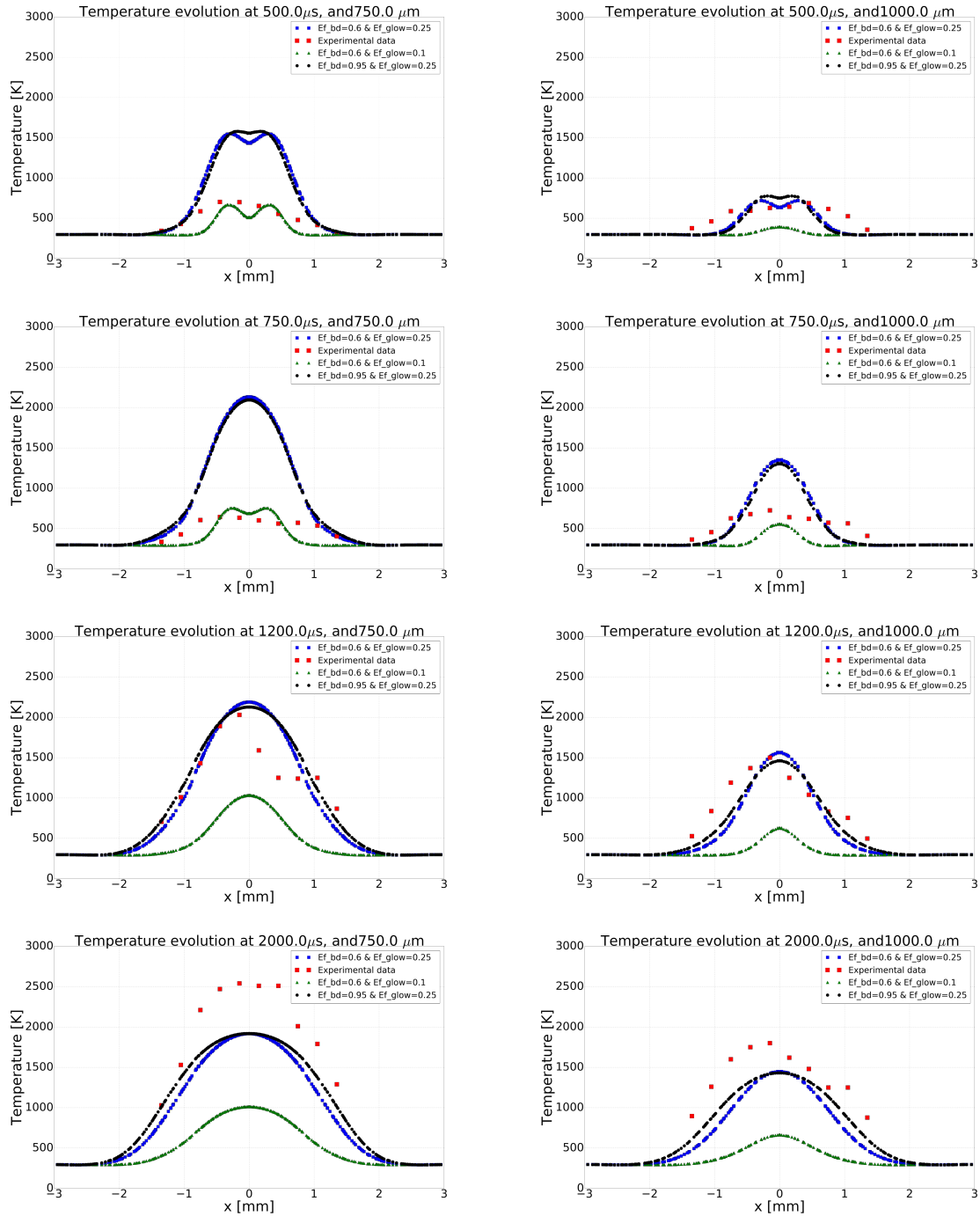
Figure 17: Comparison with experimental data of temperature evolution versus the width at different heights ($750\mu m$ and $1000\mu m$) and times ($5000m$ and $10000m$) of the simulation in pure air without chemical effect

After this peak of temperature, for each case, the temperature strongly decreases for a strong breakdown efficiency and slightly decrease with a low breakdown efficiency. Then, around $100\mu s$ for High_Bkd and around $110\mu s$ for Low_Glow, the temperature increases until almost $2800K$ for both around $0.1ms$. After $0.1ms$, the temperature is equal with a strong or a low breakdown efficiency. For the other points, temperatures are slightly lower but results are similar.

Eventually, the breakdown phase has only an impact on the early stages of the ignition, during approximately the first millisecond and its effect on the latter time is minor. Moreover, the breakdown creates a first peak of temperature which is confirmed by experimental data. This temperature then decreases until $100\mu s$ and increases because of the glow phase which delivers enough energy by diffusion and convection. Furthermore, to validate the fact that the breakdown phase has a minor effect on latter times, the Fig. 18 shows few differences between curves with a strong or weak breakdown efficiency.

Impact of the energy transfer efficiency of the glow phase on ignition The glow phase only happens after the breakdown so its study is only relevant after $20ns$. Moreover, as presented in Fig. 16, the second peak of temperature starts around $100\mu s$. The study of Fig. 18 is then made with curves from $500\mu s$ to $2000\mu s$.

On this Fig., at every presented time ($500\mu s$, $750\mu s$, $1200\mu s$ and $2000\mu s$), and at every presented heights, the temperature with a low glow efficiency is lower than with a bigger efficiency. At $1200\mu s$ and $750\mu m$, for a bigger glow efficiency, the temperature is around $2200K$ and around $1000K$ for a lower glow efficiency.

Furthermore, at $500\mu s$, the Ref curve and the High_Bkd curve present an hole of temperature around x=0 mm. This hole of temperature is due to the formation of the torus and is slowly filled by the energy diffused by the glow.

Finally, the energy delivered by the glow phase by diffusion and conduction is important for the end of the ignition because it is from this energy that the hot kernel gas will expand.

Figure 18: Comparison with experimental data of three different temperature evolutions versus the width at different heights ($750\mu m$ and $1000\mu m$) and times ($500\mu s$, $750\mu s$, $1200\mu s$ and $2000\mu s$)

8   Conclusion and perspective

For this paper, four DNS of an anode-cathode configuration have been performed. Two simulations concerns a discharge in pure air and two other one concerns a discharge in a propane/air mixture at $\phi = 1$. For each discharge, an ignition model is used and two differents chemical mechanisms are compared.

The comparison of simulations with and without plasma chemistry shows big temperature differences in the early stages of the ignition for discharge in pure air and in a propane/air mixture. As described in the result part, these differences are mainly due to dissociations and recombinations of the dioxygen and of the dinitrogen. The chemistry of the dissociation and of the recombination of the dioxygen exists in the combustion chemistry. So the use of this combustion chemistry already allows to get some differences of temperature for this simulation with dissociations of dioxygen. Finally, after approximately $2\mu s$, both simulations with and without the plasma chemistry are similar so this plasma chemistry is specially important for early stages of the ignition.

Those simulations are also compared to experimental data. They show some differences on the temperature fields. Those differences are due to numerical parameters such as the diameter of the energy deposition model that should be better calibrated for future simulations. Some hypothesis also need to be modified such as the symmetry hypothesis between both electrodes. Experimentally, an asymmetry is presented and the used of a truncated cone might take into account this asymmetry.

Finally, this chemistry description methodology with this energy deposition model seems promising even if a better calibration of the energy deposition model has to be done for industrial studies.

9 Bibliography

[1] European Parliament and Council of the European Union. REGULATION (EU) No 333/2014 OF THE EUROPEAN PARLIAMENT AND OF THE COUNCIL of 11 March 2014 amending Regulation (EC) No 443/2009 to define the modalities for reaching the 2020 target to reduce CO 2 emissions from new passenger cars THE. *Official Journal of the European Union*, (333):15–21, 2014.

[2] Rudolf Maly and Manfred Vogel. Initiation and propagation of flame fronts in lean ch4-air mixtures by the three modes of the ignition spark. In *Symposium (International) on Combustion*, volume 17, pages 821–831. Elsevier, 1979.

[3] M. Kono, K. Niu, T. Tsukamoto, and Y. Ujiie. Mechanism of flame kernel formation produced by short duration sparks. *Symposium (International) on Combustion*, 22(1):1643–1649, 1989.

[4] G.Lacaze. *Large Eddy Simulation of the ignition of cryogenic rocket engine.* PhD thesis, INP Toulouse, CERFACS, 2009.

[5] E Sher, J Ben-Ya'ish, and T Kravchik. On the birth of spark channels. *Combustion and flame*, 89(2):186–194, 1992.

[6] C. Becerril. Étude des systèmes d'allumage: De l'étincelle à la flamme. 2013.

[7] Dario Maestro. Ignition fundamentals for internal combustion engines. 2014.

[8] R. Mendez-Rojano. Study of spark plug ignition. 2015.

[9] Michael J Zehe, Sanford Gordon, and Bonnie J McBride. Cap: A computer code for generating tabular thermodynamic functions from nasa lewis coefficients. 2001.

[10] A. D'Angola, G. Colonna, C. Gorse, and M. Capitelli. Thermodynamic and transport properties in equilibrium air plasmas in a wide pressure and temperature range. *European Physical Journal D*, 46(1):129–150, 2008.

[11] AVBP Chemistries. Two steps mechanism : Cm2 (300k, 1bar). `http://www.cerfacs.fr/~avbp/AVBP_V6.X/AVBPHELP/PARAM/chemistry/Air/ch4/2s/cm2/index.php`.

[12] Ramanan Sankaran, Evatt R. Hawkes, Jacqueline H. Chen, Tianfeng Lu, and Chung K. Law. Structure of a spatially developing turbulent lean methane-air Bunsen flame. *Proceedings of the Combustion Institute*, 31 I:1291–1298, 2007.

[13] B Franzelli. *Développement de cinétiques chimiques réduites pour la simulation aux Grandes Echelles de foyers aéronautiques.* PhD thesis, PhD thesis, INP Toulouse. 225, 248, 2011.

[14] Tianfeng Lu and Chung K. Law. Reduced mechanisms download. 2015. `http://www.engr.uconn.edu/~tlu/mechs/mechs.htm`.

[15] T. Kravchik, E. Sher, and J. B. Heywood. From Spark Ignition to Flame Initiation. *Combustion Science and Technology*, 108(1-3):1–30, 1995.

[16] Rudolf Maly. Ignition model for spark discharges and the early phase of flame front growth. *Symposium (International) on Combustion*, 18(1):1747–1754, 1981.

[17] T. Poinsot and D. Veynante. Theoretical and Numerical Combustion. *Combustion and Flame*, 32(1):534, 2005.

[18] F Collin, B Cuenot, E Riber, O Vermorel, A Cayre, S Richard, A Misdariis, and P Champeix. DNS of spark-ignition in an anode-cathode configuration: impact of plasma chemical kinetics. 2017.

[19] Perrine Pepiot. *Automatic strategies to model transportation fuel surrogates*. Stanford University, 2008.

[20] Ph Teulet, J J Gonzalez, A Mercado-Cabrera, Y Cressault, and A Gleizes. One-dimensional hydro-kinetic modelling of the decaying arc in air–pa66–copper mixtures: Ii. study of the interruption ability. *Journal of Physics D: Applied Physics*, 42(18):185207, 2009.

[21] S Gordon and B McBride. Chemical Equilibrium with applications. 1996. `https://cearun.grc.nasa.gov/`.

[22] T. Poinsot and S.K. Lele. Boundary conditions for direct simulations of compressible viscous flows. *Journal of Computational Physics*, 101:104–129, July 1992.

10 List of Figures

11 Appendices

11.1 Review of the ignition's kinetic : Lu results and analysis

Figures 19, 20 and 21 show that a propagative flame is created around the shock as predicted with the CM2 scheme and the mesh resolution is not efficient enough to resolve the flame front.
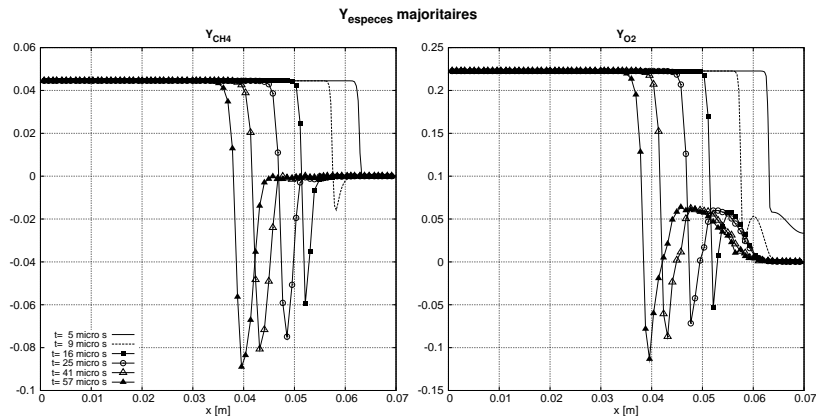
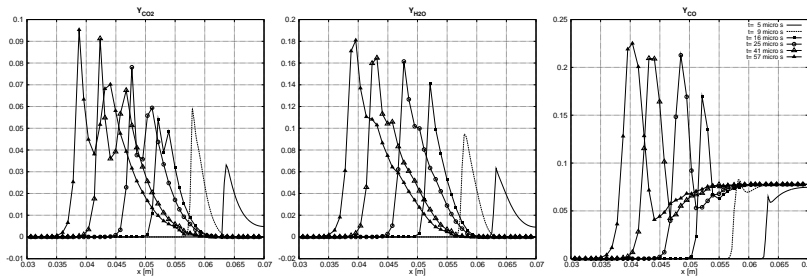Figure 19: Reagents evolution during the simulation with a Lu scheme.

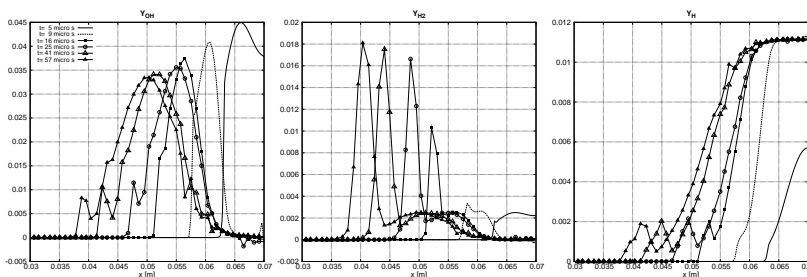Figure 20: Products evolution during the simulation with a Lu scheme.

Figure 21: Some intermediate species evolution during the simulation with a Lu scheme.

With 73 reactions, it will be complicate to expose every reagents and products evolution. Only more significant reaction rates are presented.

Every reaction rate shows that chemical reactions occur around the shock, which is the inverse with CM2 simulation.

Figures 22 and 23 presents the production of CH, CO, H_2 and H.

Reactions 3, 20, 40 and 41 are respectively :

$$O + H_2 \leftrightarrow H + OH$$

$$H + O_2 \leftrightarrow O + OH$$

$$OH + H_2 \leftrightarrow H + H_2O$$

$$2OH \leftrightarrow O + H_2O$$
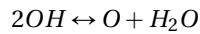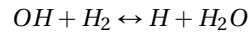
The complementary contribution of the analytic kinetic of Lu is the apparition of radicals of combustion.
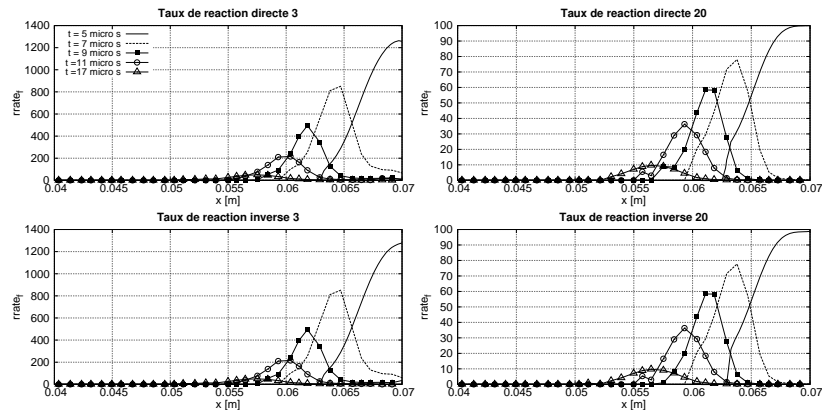
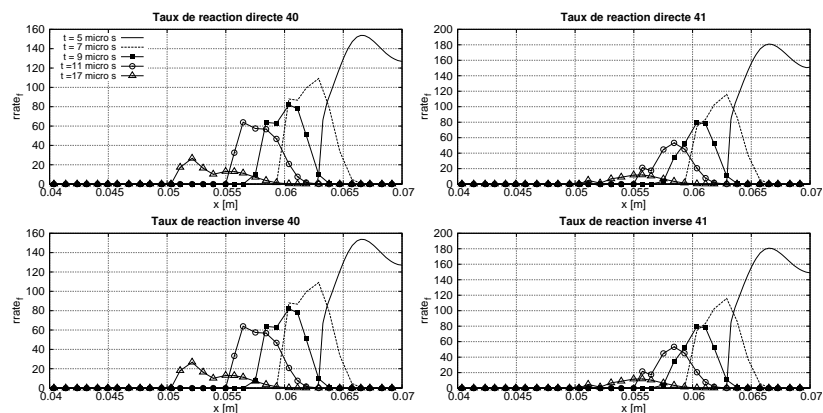Figure 22: Reaction rate during the simulation with a Lu scheme.

Figure 23: Reaction rate during the simulation with a Lu scheme for other reactions.

11.2 Review of shock waves effects on the ignition : Comparison of the pressure with the simulation of Kravchik and the simulation of Maestro

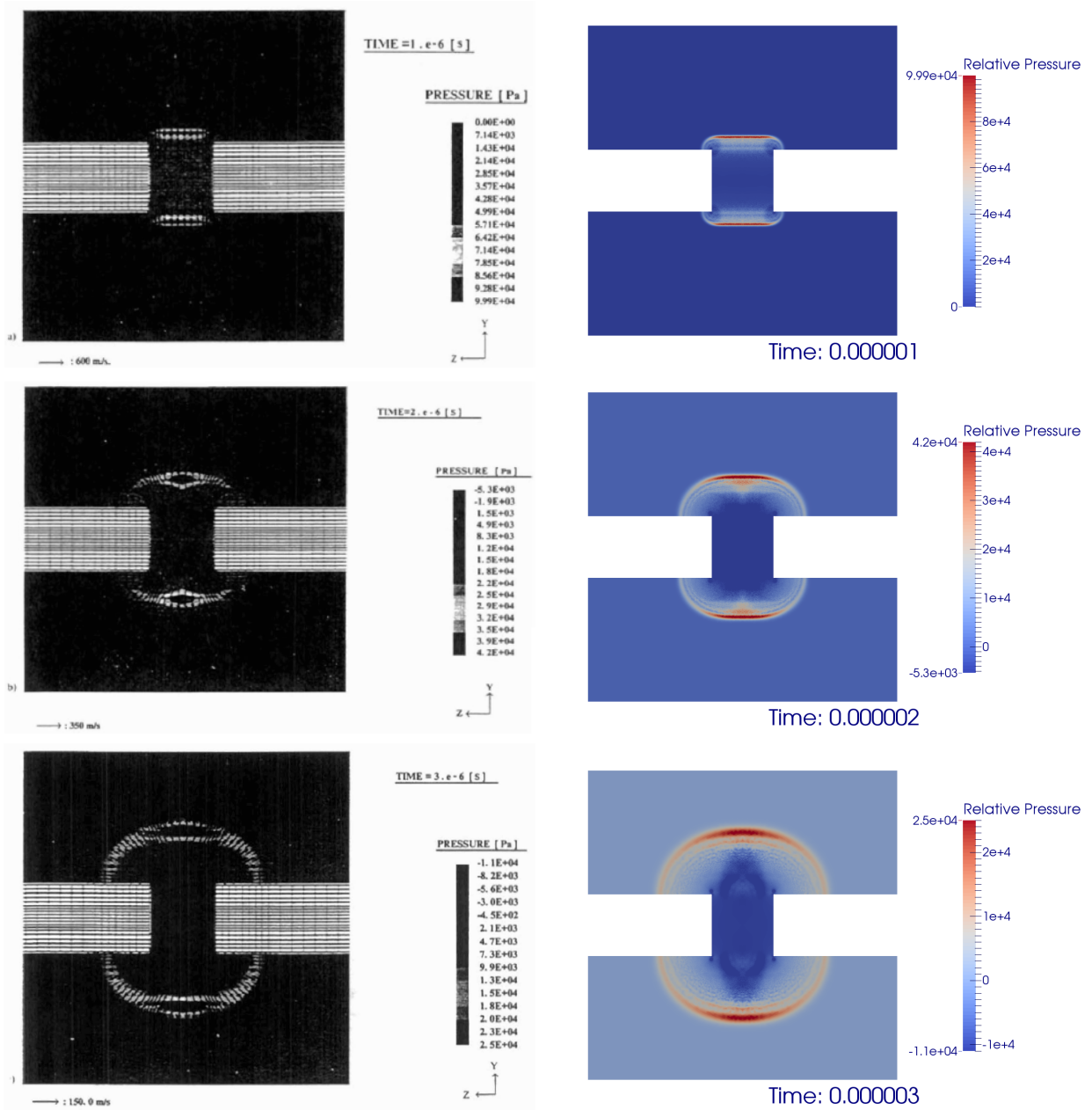**For figures from 24 to 25 :** Left image : Kravchik simulation. Right image : Maestro simulation.

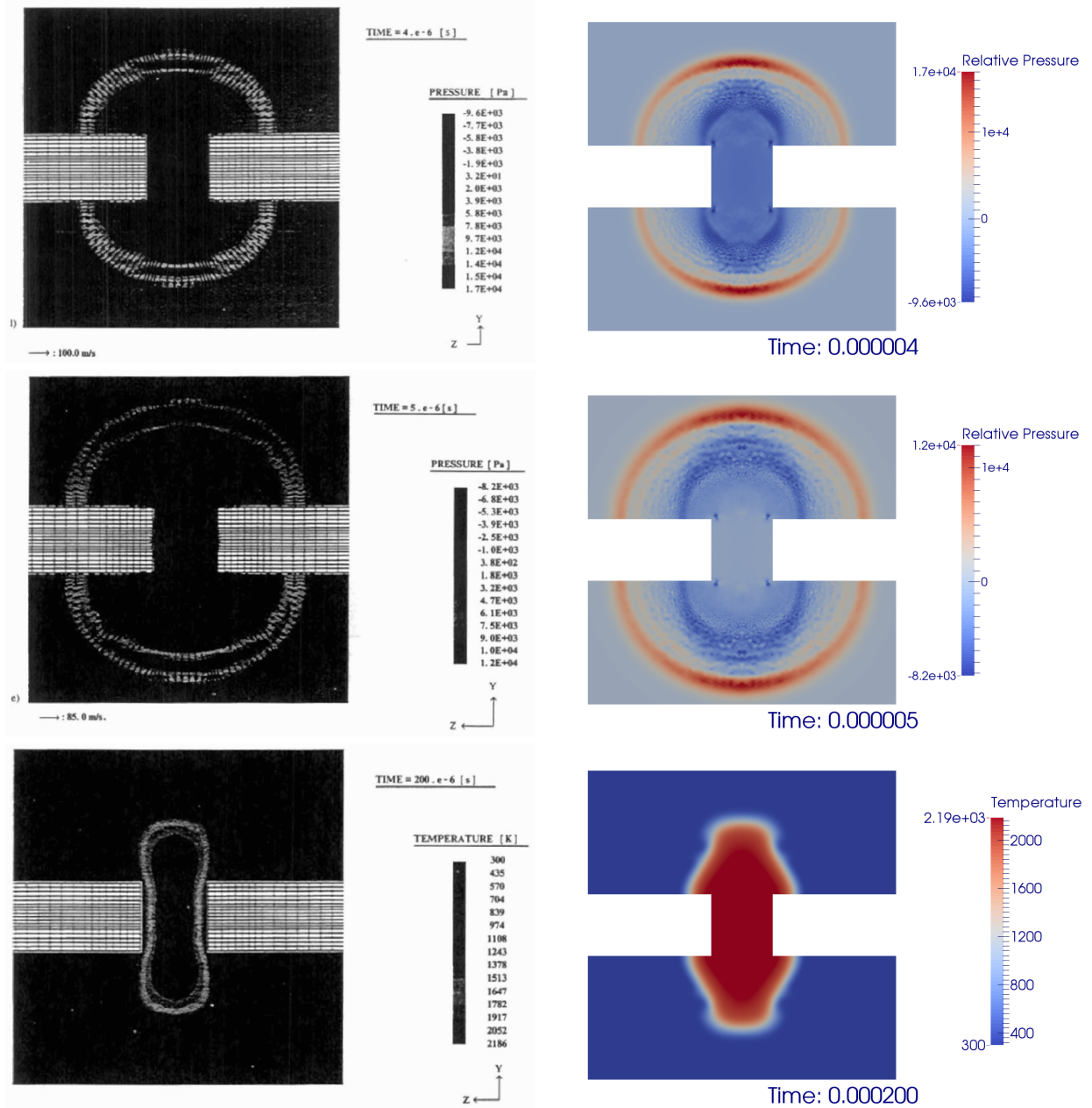Figure 24: Field of relative pressure at $t = 1\mu s$, $t = 2\mu s$ and $t = 3\mu s$.

Figure 25: Field of relative pressure at $t = 4\mu s$, $t = 5\mu s$ and $t = 200\mu s$.